Advances in Science and Technology Research Journal

*Advances in Science and Technology Research Journal*, 2025, 19(9), 92–104
https://doi.org/10.12913/22998624/205997
ISSN 2299-8624, License CC-BY 4.0

Received: 2025.05.06
Accepted: 2025.07.15
Published: 2025.08.01

# Effect of heat input on distortion and morphology of tungsten inert gas welded joints in AISI 304L stainless steel

Anna Szewczyk[1*], Roksana Jarska[2], Grzegorz Rogalski[1]

[1] Institute of Manufacturing and Materials Technology, Faculty of Mechanical Engineering and Ship Technology, Gdańsk University of Technology, Gabriela Narutowicza Street 11/12, 80-233 Gdańsk, Poland
[2] Eaton Truck Components Sp. z o.o., 30 Stycznia 55, 83-110, Tczew, Poland
* Corresponding author's e-mail: anna.szewczyk@pg.edu.pl

## ABSTRACT

Due to the physicochemical properties of austenitic stainless steels, their welding may result in significant joint distortions and adverse microstructural changes, leading to the formation of unacceptable welding imperfections. This study investigates three single-pass fillet welding techniques employing the tungsten inert gas (TIG) process (141) for joining AISI 304L austenitic stainless steel sheets. It was found that the use of lower heat input value does not cause discoloration of the weld. Moreover, it was observed that reducing the parameters causes the vertical sheet metal to deflect by about 0.333° in the direction opposite to the weld. The highest heat input value caused a deflection of 4.833° towards the weld. Increasing the parameters also deflected the incoming sheet metal towards the weld, but the angle was smaller i.e. 2.167°. An inadequate ferrite content was observed in the specimen welded under the lowest parameter settings. Macroscopic examination revealed no significant welding imperfections. Microscopic analysis showed a microstructure characteristic of the materials used. The width of the heat-affected zone varied with the applied parameters, increasing with higher heat input. The study demonstrated that parameter selection significantly influences the properties of the resulting joint. In developing the welding procedure for AISI 304L austenitic stainless steel, particular emphasis should be placed on controlling heat input, as it is the primary factor determining both the joint properties and the magnitude of welding distortions.

**Keywords:** austenitic stainless steel, TIG welding, angular distortion, ferrite measurement.

## INTRODUCTION

The continuous advancement of industry and the growing demand for materials necessitate a deeper understanding of available iron alloys and the expansion of their potential applications. Consequently, the demand for steel has been steadily increasing over time. Stainless steels can be distinguished here, the production of which is constantly growing, as well as steels from new classes of materials which are, generically, called high-entropy alloys (HEA) [1,2]. However, due to price, availability and also easier processing, stainless steels are still commonly used group of materials. This is owing to the attractiveness of this group of steels resulting from their properties, which allow them to be used in practically every industry, as well as the increase in anti-corrosion requirements, failure-free operation of devices and the desire to reduce the costs of maintaining and operating machines and structures [3,4].

Among the types of stainless steel, austenitic stainless steels occupy a special place. This is due to their versatility, which allows them to be used in numerous industries, i.e. wherever corrosion resistance, hygiene, durability and ease of processing and forming are required [5–7]. It can be mentioned: food industry – production of food storage containers, kitchen tools and food processing equipment; chemical industry – production of tanks, pipelines, heat exchangers and other devices; medical industry – surgical and dental tools, implants; automotive industry – production of exhaust elements, fuel tanks, fastening elements;

petrochemical industry – tanks, pipelines, devices in contact with aggressive environments [7–11]. Like other steel grades, they contain a small amount of carbon and a relatively large amount of chromium. Additionally, they include nickel, which is the basic austenite-forming element. The most common types of austenitic stainless steel are classified as group 300 according to the AISI/ASTM standard, i.e. chrome-nickel or chrome-nickel-molybdenum. Among the undoubted advantages of austenitic steels, which make them attractive, can be found high corrosion resistance, good mechanical properties and high susceptibility to cold forming [7,12,13]. It should be noted that they are characterized by the highest impact strength values in a wide temperature range among all stainless steel grades. Problematic, especially during welding, are the high coefficient of thermal expansion and the low coefficient of thermal conductivity defining this type of material [13]. Additionally, it is not easy to determine the weldability of these steels. Austenitic steels are generally considered to be well weldable, but incorrect selection of the parameters of welding process may lead to the formation of hot cracks, crystallization cracks in the weld, segregation cracks in the HAZ (heat affected zone), annealing cracks, as well as a decrease in impact strength and increased susceptibility to intergranular corrosion, resulting from precipitation processes and the formation of σ phases [14–16]. Therefore, it is extremely important to correctly develop the welding technology for this material. Therefore, the latest research focuses on controlling welding parameters and conditions, as well as their influence on joint properties. These issues concern both stainless steels and other types of steel grades [17–22].

TIG (tungsten inert gas) welding is a joining process using a non-consumable electrode in an inert gas shield, which is very versatile technologically and metallurgically, but is characterized by low efficiency [23,24]. It is used to make joints from virtually all material groups, but also dissimilar and combined ones [25–27]. Low efficiency requires modification of the process to increase the amount of weld metal produced, e.g. hot wire welding and A-TIG (welding with the use of an activating flux) [28–31].

Rao and Deivanathan's research confirms that the properties of welded joints, such as tensile strength and bending strength, depend on the applied current intensity. Additionally, they also point out that the parameters that allow obtaining the desired properties change depending on the consumable used – so there are no universal current values [32]. Korinko and Malene also emphasize the difficulty of welding austenitic steels due to the susceptibility of these steels to the formation of two distinct weld defects, solidification cracking and lack of penetration [33]. Sun and Han indicate that only the weldments produced using the appropriate procedure exhibit satisfactory mechanical properties, particularly toughness. They also draw attention to the control of welding parameters, especially when good resistance to hot cracking is desired [34]. Costanza et al. focused on studying the effect of shielding gases on the properties of welded joints. They concluded that the use of different shielding gases also affects the properties of joints, although not to the same extent as the selection of parameters. According to their studies, the greatest uniformity of the microhardness profile of welded cross-sections can be achieved by using a mixture of 98% Ar and 2% $H_2$ or 95% Ar, 4% $CO_2$ and 1% $H_2$, or pure argon as a shielding gas. Mixtures such as: 95% Ar + 5% $H_2$, 75% Ar + 20% He + 5% $H_2$, or 90% Ar + 8% $CO_2$ + 2% $O_2$ caused greater imperfections, which directly translates into strength properties [35]. The influence of shielding gases on the properties of joints was also studied by Durgutlu, who found that the addition of $H_2$ to Ar increased the tensile strength. In addition, the penetration depth and bead width increased with the increase in the hydrogen content in the shielding gas, as did the average grain size in the weld metal [36]. Varbai reached similar conclusions, but he studied the effect of adding nitrogen and oxygen to argon [37]. These studies show how difficult and important it is to use appropriate welding parameters to obtain the required strength properties, and also draw attention to the need to deepen knowledge about the influence of welding variables on the final result. However, it is worth developing research on TIG welding, as emphasized by scientists in their studies [38–40], especially since this method can be successfully used not only for welding similar steels, but also for joining materials with different microstructure and properties [41,42], and even for regenerating the damaged surface of composite materials [43].

Therefore, the objective of this article is to examine the influence of welding parameter selection, and consequently heat input, on the welding distortions and morphology of joints welded from 304L austenitic stainless steel using the TIG method.

## MATERIALS AND METHODS

For the tests, sheets of 304L austenitic stainless steel (1.4307; material group 8.1 according to TR ISO 15608) were used as the base material. This grade of steel has a lower carbon content than AISI 304 and is widely used in industry. The material, with sheet dimensions of 2 × 88 × 137 mm, was provided in a hot-rolled, annealed, pickled and smoothed condition, meeting the 2B finish standards. The composition of the steel used, which is known from the material certificate provided by the material supplier, is presented in Table 1.

The manual TIG (141) method was selected to join the sheets using a Lincoln Electric Invertec 400 TPX welding machine. As a filler metal, it was decided to use a solid rod with a diameter of 1.6 mm, marked according to ISO 14343-A W 19 12 3 L Si, which is an austenitic welding rod with a reduced carbon content and a simultaneous increase in the percentage of silicon. The composition of the consumable was determined based on the wire manufacturer's catalog and is presented in Table 2. Argon (Ar) according to PN-EN ISO 14175 was used as the shielding gas, with a flow rate of 8 l/min. There was no backing gas. The tungsten electrode type was WL15 and its diameter was 2.4 mm. The nozzle diameter was 12 mm. Direct current with negative polarity (DC-) was applied. Prior to initiating the welding process, three 2 mm long TIG tack welds were made at the beginning, end, and center of each sample.

Three T-joints with single-pass fillet welds were welded (FW sl) in PB position, therefore, three welding technological instructions were developed, characterized by different parameters that translate into the heat input which is shown in Table 3.

The achievement of the set goal was accomplished based on the following research plan:

1. Development of welding technology (WPS – welding procedure specification).
2. Weld of test joints and preparation of samples for testing according to the prepared test plan (Table 3).
3. Performing non-destructive tests:
   - visual tests (VT);
   - penetrant tests (PT);
   - angular distortion measurements;
   - measurements of the volume fraction of high-temperature ferrite
4. Performing destructive tests:
   - macroscopic metallographic examinations;
   - microscopic metallographic examinations.

Penetrant testing was carried out using remover, penetrant and developer manufactured by OPN CHEMIE company. After cleaning and drying the welded joints, the penetrant was applied and left for about 10 minutes. Excess penetrant was then removed and developer was applied. To measure the angular distortion, a universal analogue angle meter MKMb with a measuring range of 0–360° and an accuracy of 0°05′ was used. The measurement was performed at three points, allowing to obtain information about the deformation along the entire length of the welded joint – at the beginning, in the middle and at the end of the sample, on the opposite side the weld. It was decided to take three measurements, because it was considered that such a number would be sufficiently representative of the entire joint. The tested sample is relatively short, and the points that were selected represent the most critical locations (the beginning of the sample, which is characterized by instability of parameters due to arc ignition, the end similarly with the difference that the

**Table 1.** 304L austenitic stainless steel chemical composition

| Element | C | Si | Mn | P | S | Cr | Ni | N |
|---|---|---|---|---|---|---|---|---|
| wt. % | | | | | | | | |
| Content | 0.015 | 0.38 | 1.54 | 0.029 | < 0.001 | 18.10 | 8.00 | 0.052 |

**Table 2.** W 19 12 3 L Si welding wire chemical composition

| Element | C | Mn | Si | Cr | Ni | Mo |
|---|---|---|---|---|---|---|
| wt. % | | | | | | |
| Content | 0.03 | 1.9 | 0.8 | 18.5 | 12.0 | 2.7 |

**Table 3.** Welding parameters of test joints

| Sample number | Welding current I [A] | Arc voltage U [V] | Welding time t [s] | Welding speed v [mm/s] | Heat input Q [kJ/mm] |
|---|---|---|---|---|---|
| S1 | 66 | 11.6 | 150 | 0.9 | 0.51 |
| S2 | 125 | 12.2 | 90 | 1.5 | 0.61 |
| S3 | 180 | 17.3 | 30 | 4.6 | 0.41 |

variability of parameters results from arc extinction, and the center of the joint as a location from a stabilized process). Ferrite content was measured using a Feritscope Fisher MP30 with a measuring head that was applied eight times to each of the three designated sample zones (base material – BM, heat-affected zone – HAZ and weld material – W), and then the average content and standard deviation were calculated. Ferrite content was measured in three different zones of the weld to investigate and compare its distribution depending on the location, with the aim of better understanding the structural changes within the joint. Macroscopic tests were performed on prepared samples, which were first cut using a band saw, then ground and etched with a reagent made of nitric acid, hydrofluoric acid and distilled water. In order to obtain the possibility of observation under a microscope, the previously prepared sections were embedded in resin and then ground down, polished and etched with the same reagent used when preparing samples for macroscopic examination. An Olympus BX-52 microscope was used to observe the samples.

## RESULTS

### Non-destructive testing

Visual tests were performed on all samples, along the entire length of the weld, in accordance with the guidelines of the PN-EN ISO 17637 standard. Traces of silicon from the welding consumables used were observed at the S1 weld. Moreover, the tested joint was characterized by high purity with no visible traces of oxidation. On the remaining two samples (S2, S3) numerous tarnish colours were noted, probably caused by the release of iron oxides. Photos of the completed joints are shown in Figure 1. What is more, the insufficient material addition in relation to the used parameters resulted in undercutting at the ends of the last two samples and a crater at the end of the S3 joint.

Penetrant tests did not reveal any surface weld imperfections for all samples. They only confirmed the occurrence of defects at the ends of S2 and S3 joints observed during visual tests. Photos of samples after penetrant testing are shown in Figure 2.

Angular distortion was defined as the deviation of the plates from their original position, which was equal to a right angle. It was measured at three points and the average of the measurements obtained for the sample S1 was 0.333°, S2 – 4.833° and S3 – 2.167°. The measurement results are presented in Table 4. It is worth noting that the change in the angular position of the first tested element (S1) has the opposite sign to the other two, i.e. the deviation occurred in the opposite direction and an obtuse angle was obtained. However, an acute angle was created for S2 and S3 ($\alpha < 90°$).

The results obtained are extremely interesting when compared with the parameters with which the samples were welded, as well as with heat input. They show that a joint made with the highest heat input is characterized by the highest deflection. Interestingly, however, the sample with the lowest heat input during welding did not obtain the smallest angular distortion. This value distinguishes the welded joint with the lowest parameters, and additionally in its case the deflection occurred in the opposite direction than in the case of the other samples.

The results obtained during the ferrite content test and their standard deviation are presented in Figure 3. It is worth noting that in accordance with the PN-EN ISO 8249 standard specifying the minimum ferrite content, the amount of this structure is consistent with the requirements for the S2 and S3 samples. For the S1 lower than desired values were obtained, which may be the result of incorrectly selected parameters and reduce the joint's corrosion resistance and resistance to hot cracking.


**Figure 1.** View of the joints of samples a) S1, b) S2, c) S3

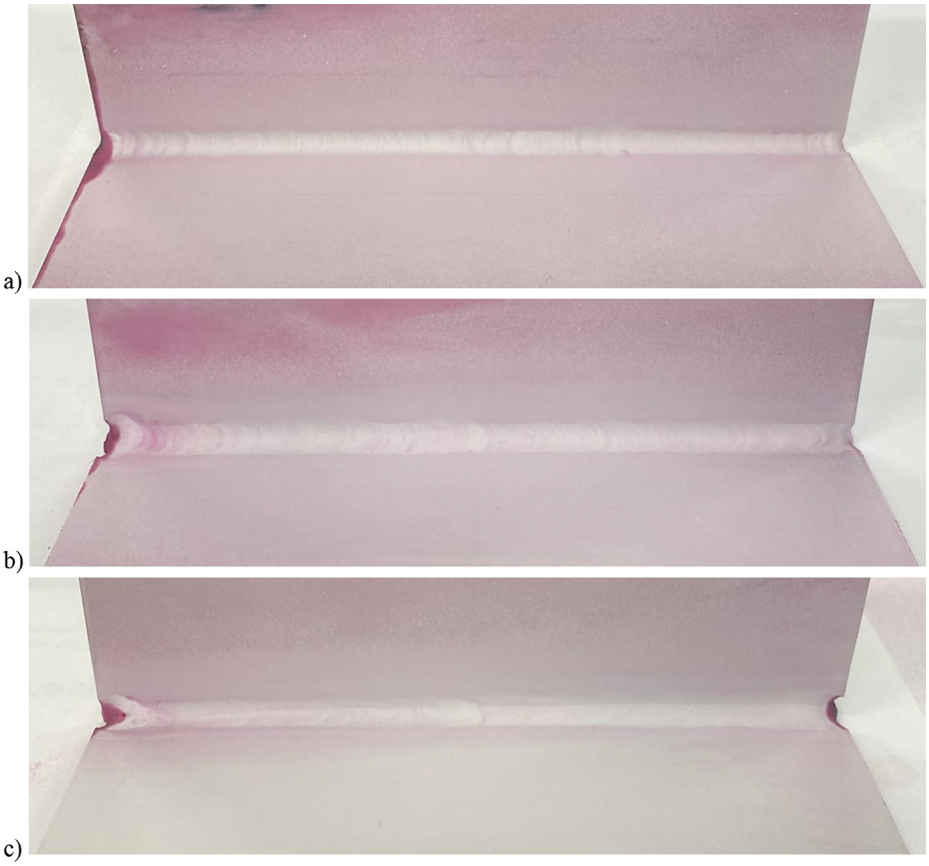


**Figure 2.** View of the joints of samples after penetrant testing a) S1, b) S2, c) S3

**Table 4.** Results of angular distortion measurements of made test joints

| Measuring point | Weld sample S1 | | Weld sample S2 | | Weld sample S3 | |
|---|---|---|---|---|---|---|
| | The value of the measured angle | Deflection value α | The value of the measured angle | Deflection value α | The value of the measured angle | Deflection value α |
| 1 | 91.000° | 1.000° | 84.500° | 5.500° | 88.000° | 2.000° |
| 2 | 90.000° | 0.000° | 85.500° | 4.500° | 88.000° | 2.000° |
| 3 | 90.000° | 0.000° | 85.500° | 4.500° | 88.500° | 2.500° |
| Average | 90.333° | 0.333° | 85.167° | 4.833° | 88.167° | 2.167° |

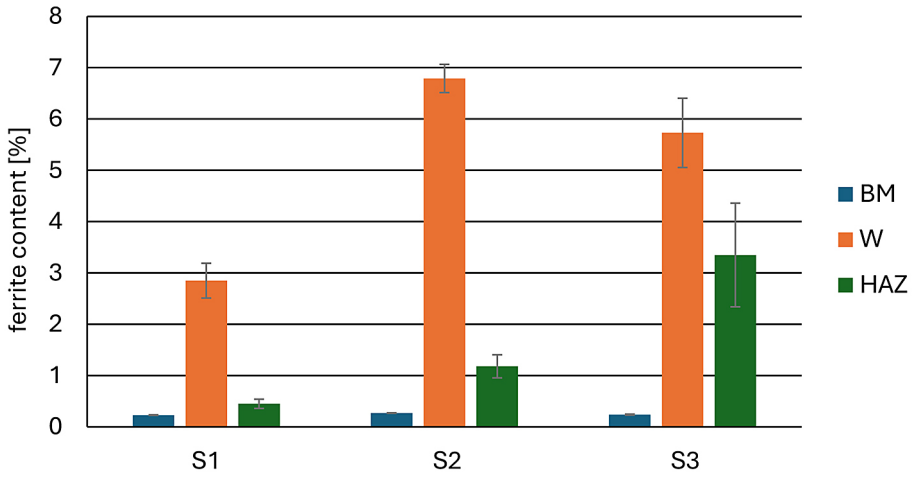


**Figure 3.** Average values of the ferrite content

## Destructive testing

The samples shown in Figure 4 were subjected to macroscopic tests. They allowed to determine that none of the joints had any undercuts, lack of fusion, cracks, non-metallic inclusions or porosity. Moreover, it was noticed that all samples were characterized by a concave face, with a smooth transition into the base material of the joined elements. The first and second welds are symmetrical, but the penetration obtained when welding the second element is deeper. What is more, it may seem that in S1 there was no full penetration (no fusion was achieved), however, after analysis using the ImageJ program it was found that minimal fusion was achieved, which was confirmed by subsequent microscopic examination. Nevertheless, it does show that while structural integrity exists, in terms of strength properties the test may deviate significantly from the values obtained for the other samples. In the case of sample S2, it may seem that the weld is a multi-pass weld. However, this is only apparent, and this illusion is related to the welding technique and parameters, which directly translates into the material solidification process. The heat input in this case caused the accumulation of dendrites in the lower part of the weld, which in turn affected the way the material was etched, resulting in the illusion of a two-pass welding. Additionally, there is a noticeable deviation of the vertical plate towards the weld, which makes it stand out from other joints in which the change in angular position occurred towards the weld. The third sample differs from the others in terms of geometry - the weld is large and asymmetrical, and the welder melted a thin plate. The HAZ is so narrow that it was impossible to observe it during macroscopic examination.

The analysis of the microstructures of the base materials showed a typically austenitic structure with small, regular grains and visible twin formations. The heat-affected zone of sample S1 is characterized by small dimensions (50–100 μm) and the presence of high-temperature δ ferrite arranged in zones. The last band of ferrite occurring in this zone is the fusion line below which there are expanded austenite grains. The HAZ of the sample S2 is noticeably wider (70–200 μm) and is characterized by overheating and

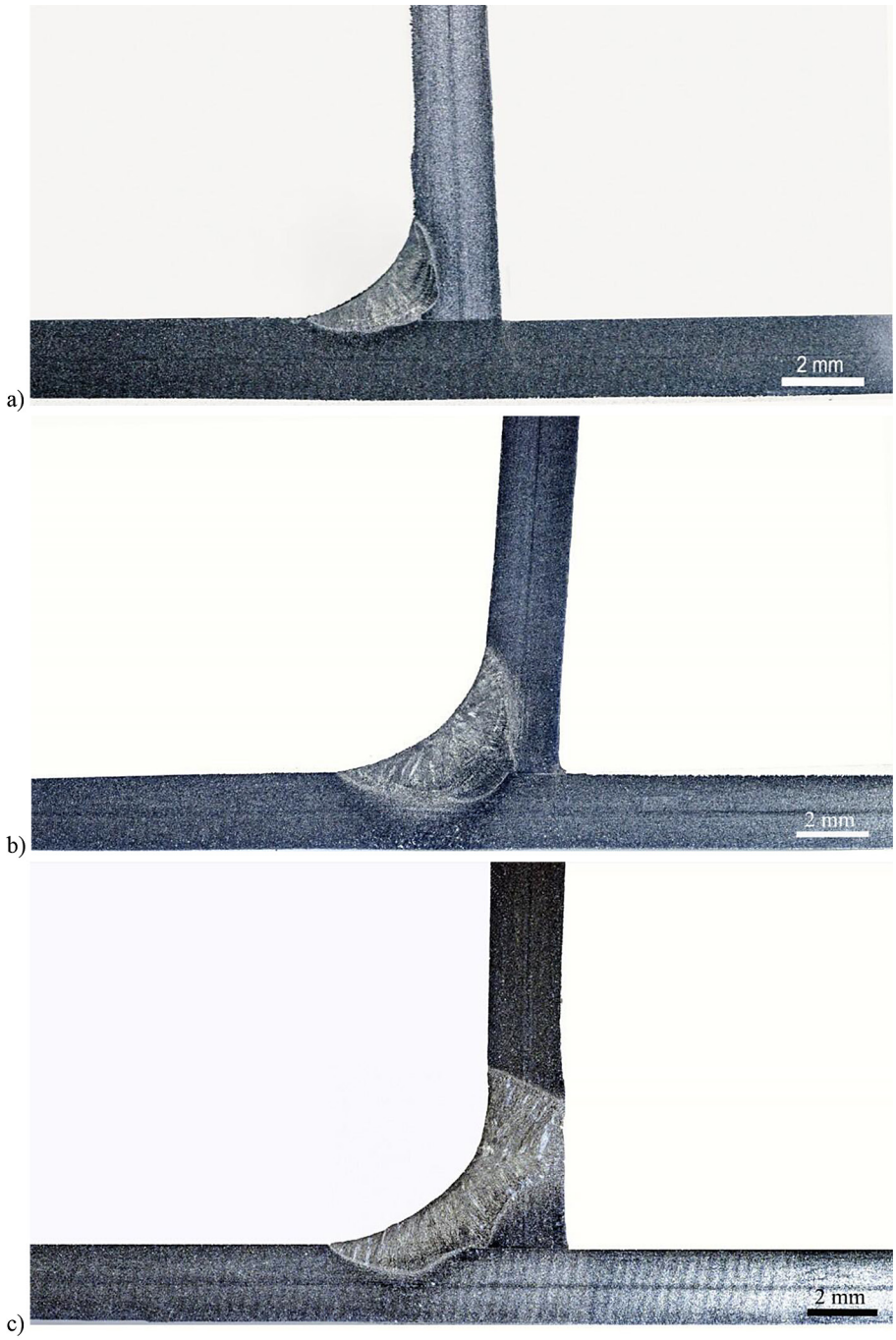


**Figure 4.** Cross-sections of welded joints: a) S1, b) S2, c) S3

local thickening of high-temperature ferrite appeared, which has a spherical structure on the fusion line. The HAZ of the third sample (S3) is narrow (approximately 100 µm) and, as in the case of the previous joints, there is high-temperature ferrite, which is characterized by a globular shape on the fusion line. Dendrite axes turning into coarse-grained austenite grains also appeared. As in the first sample, they changed. In the case of weld materials of all samples, observations revealed dendritic structures composed of austenite with high-alloy ferrite precipitates on their branches. The first joint is distinguished by the smallest amount of δ ferrite precipitates, while the largest amount can be observed in the second joint. In the third case, an even distribution of dendrites with separated high-temperature ferrite is noticeable. No chromium carbide precipitation was observed at the grain boundaries in any sample, despite the differences in heat input. Figures 5 and 6 show the analyzed microstructures of samples S1–S3.

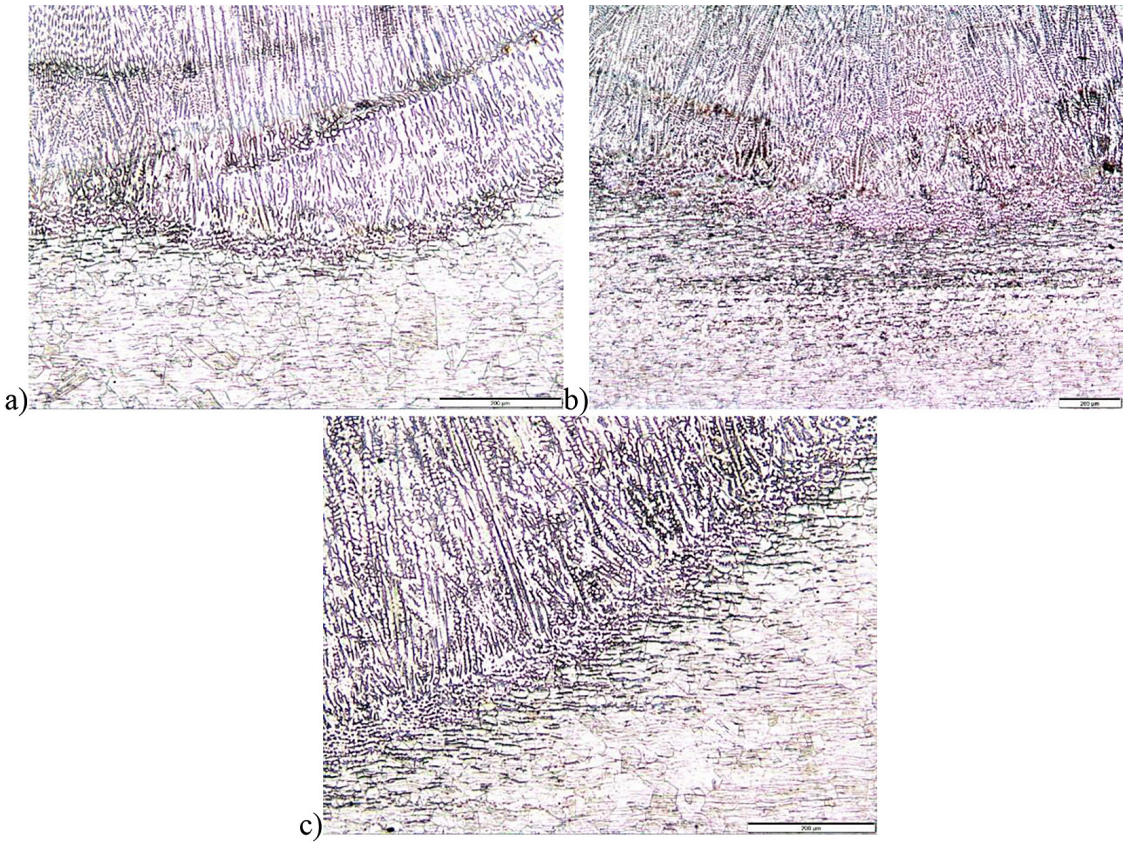


**Figure 5.** Microstructure of HAZ, magnification 100x a) sample S1, b) sample S2, c) sample S3

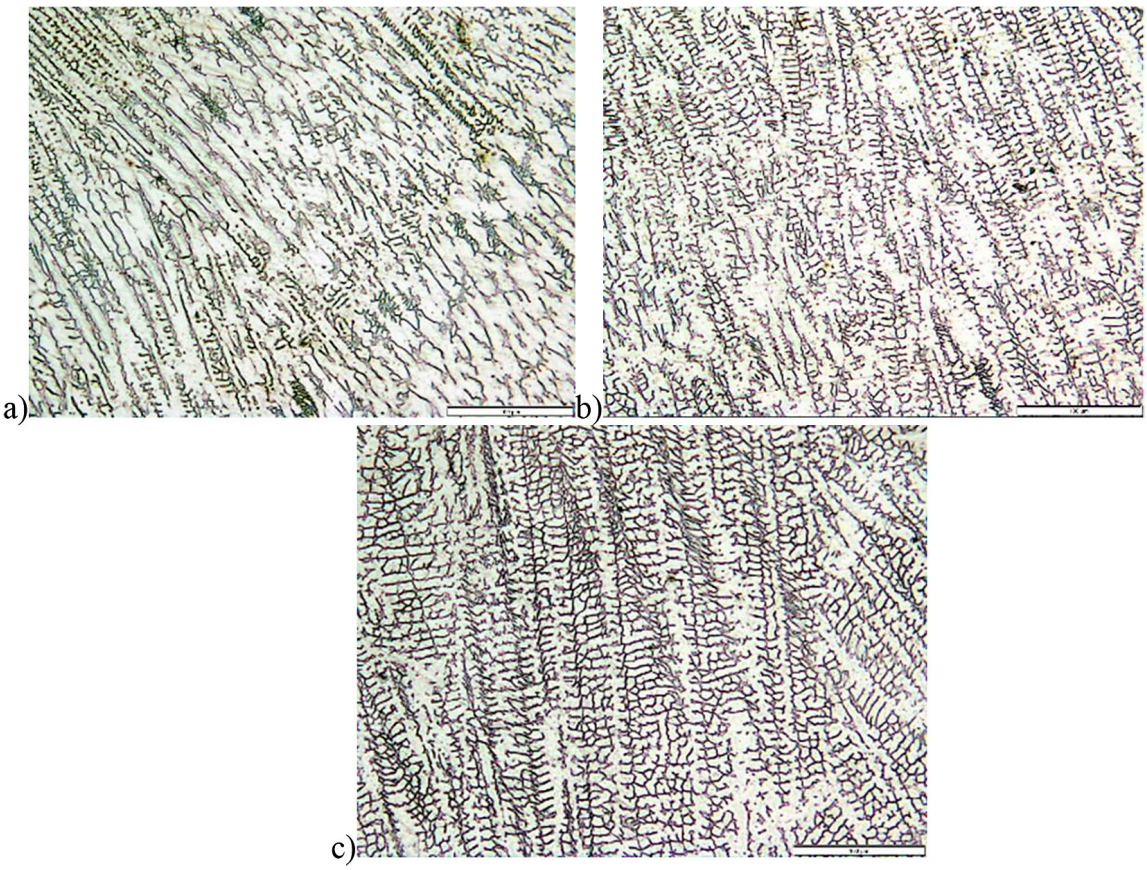


**Figure 6.** Microstructure of the weld material, magnification 200x a) sample S1, b) sample S2, c) sample S3

## DISCUSSION

The conducted studies show how the selection of parameters affects the properties of welded joints, but also that heat input does not always determine the properties of the joint. In the case of the tested samples, the difference between the heat input was 0.1 kJ/mm. It would seem that these are insignificant differences, but in comparison with the parameters used, a broader picture is obtained. The welded joint with the smallest parameters and the longest welding time (S1) was characterized by an average heat input, but low parameters result in the achievement of the smallest measured values, i.e. the smallest angular distortion and the smallest ferrite content in each of the joint zones. It is worth noting that the deflection in this sample took a different direction than in the case of the other joints. This observation is consistent with the conclusions given by Unnikrishnan et al., according to which the residual stresses at low heat input are compressive, while for higher values they are tensile [44]. Additionally, in the case of this sample, the obtained weld is not symmetrical – more additional material is present on the bottom sheet, and consequently less heat input was introduced into the vertical sheet, which may also translate into the direction and value of angular distortion. Low ferrite content, such as that found in the tested sample, may cause an insufficiently developed austenite-ferrite interface, and thus facilitate crack propagation in the last phase of crystallization [12,13]. Studies by Shankar et al. [45] and Luppo et al. [46] confirm that in the case of hot cracks, the solidification mode is extremely important, and thus the appropriate ferrite content, in order to prevent the propagation of this type of cracks. Additionally, insufficient ferrite content may cause an increase in impurities such as sulfur or phosphorus in the interdendritic liquid solution in the last phase of crystallization and create preferential conditions for the formation of hot cracks [12,13].

Sample S3 welded with the highest parameters and the shortest welding time was characterized by the lowest heat input. However, despite this, the deviation values or ferrite content are neither the smallest nor the largest. The only exception is the ferrite content in HAZ, but this may result from burning through the incoming sheet. The explanation for obtaining average values of deviations despite using the largest parameters, which could suggest the largest distortion, is that the heat input for this test had the lowest value. What is more, in order to obtain a smooth transition of the weld surface into the base material, deep penetration was obtained, which resulted in uniform and greater heat dissipation and, consequently, in obtaining a stress distribution including both compressive and tensile stresses with the predominance of the latter. Additionally, as a result of this and the use of too high welding parameters, excessively deep penetration was achieved, which almost led to burning through the material, significantly affecting the shape of the weld. The welding rod melted into the sheet, which is why the weld observed during macroscopic examination appears to be slightly concave. It is highly probable that this also affected the stress distribution within the weld, consequently contributing to the observed angular distortion. Moreover, despite the lowest heat input, it is in this sample that traces of overheating are visible, which only confirms the thesis that even despite the use of low heat input, too high welding parameters can negatively affect the properties of the joint and it is extremely important to control all welding parameters.

Sample S2, despite being welded using average parameters, is characterized by the maximum tested properties, i.e. the largest angular distortion and the largest ferrite content in the base material and the weld, which results from the largest heat input. As reported by García-García et al. [47], a higher heat input results in a direct increase in angular distortion of the joint. Similar conclusions were reached by Mousavi et al. [48], demonstrating a correlation between residual stresses and heat input. The direction of angular deformation and its value in this case result from the introduction of the highest heat input and the occurrence of dominant tensile stresses in the material, which was additionally intensified by the lower spreading of the weld and, consequently, higher point heat concentration. A high ferrite content in the joint is desirable not only for ensuring anti-corrosion protection or preventing the formation of hot cracks, but also for increasing the strength properties of the joint. During the research [49] it was proved that higher ferrite content contributes to higher tensile strength (increases ductility and mechanical strength). However, according to Muthupandi et al. [50] the amount of ferrite does not affect at all or affects very little the impact strength of the joint.

When selecting welding parameters, it is necessary to pay attention to all of them, not just to the selected ones, and also to take into account the properties of the joint that want to be obtain. Analysis of the above results allowed to conclude that the best parameters for welding a 2 mm thick austenitic sheet are the parameters used to make the second sample (S2). They will allow to obtain optimal joint properties, but in their case must be expected the deflection that must be taken into account when designing the structure. Similar parameters for sheets of similar thickness are recommended by Anand Rao et al. [32]. They found that a weld connecting 3 mm thick sheets welded with an intensity of 120 A is characterized by the best tensile strength and bending strength. Kumar et al. [51] reached similar conclusions. He indicated 120 A as the current value that allows to obtain a microstructure characterized by relatively small dendrites, which directly translates into better joint strength. He recommends the use of low heat TIG due to its good tensile strength and ductility as well as narrow HAZ and slight grain coarsening. Ghumman et al [52] distinguished the selection of parameters in relation to the desired features. In the case where one wants to obtain optimal values of microhardness or minimum surface roughness, the best choice for thin sheets (3 mm) will be to use a current of 125 A and an arc voltage of 16 V. However, if strength properties such as tensile strength and percentage elongation are more important, the most optimal values will allow to obtain parameters equal to 100 A and 16 V. They also warn against increasing the parameters, because it causes an increase in surface roughness. Similar results were also obtained during other investigations [53], also for sheet metal with a thickness of 3 mm, with the difference that the minimum surface roughness was obtained with welding parameters of 125 A and 18 V and the optimum hardness for 125 A and 20 V. Similarly to the above, reducing the current value allowed obtaining the most optimal values of ultimate tensile strength and percentage elongation, respectively 100 A, 18 V and 100 A, 16 V. However, the latest research [54] shows that in the case of identical value of heat input, welding speed and welding current do not have a significant effect on the strength, plasticity or microhardness of the joint. The authors show that the most important parameter to control during welding is heat input. What is more, researchers also note that if the smallest possible angular distortion are desired, the welding speed should be reduced, which will avoid an increase in stresses, as well as dendritic segregation and columnar crystals.

## CONCLUSIONS

Based on the analysis of the results of the conducted research, the following conclusions can be drawn:

1. The welded test joints and the tests carried out allowed for determining the influence of the basic process variables on the properties of the welded joints.
2. Visual and penetrant tests did not reveal any welding defects on the tested test joints. No geometric inconsistencies or cracks were found.
3. The highest value of average angular distortion is characteristic of the S2 joint (4.833°), which is related to the heat input, and especially the correlation between the welding speed and the welding current.
4. Ferrite δ measurements for welds in samples S2 and S3 are within the acceptance criterion (3÷15 FN). Sample S1 does not meet the specified criterion (2.85 FN). It has been shown that the heat input affects the size of the thermal impact zone (on the opposite side of the electric arc) and thus the δ ferrite content. The greater heat input, the greater the HAZ and the ferrite content δ.
5. The revealed structures in the examined joints are specific to particular areas (BM, HAZ, W). No chromium carbide precipitates were identified at the grain boundaries at the magnifications used, despite differences in the of heat input.
6. It is recommended to use welding parameters for austenitic stainless steel of 304/304L grades with a thickness of 2 mm corresponding to the range for samples S2 and S3.

## REFERENCES

1. Simion G., Mirza-Rosca J., Voiculescu I., Scutelnicu E. Corrosion behaviour of medium entropy alloy deposited on low carbon steel substrate by innovative welding method. J Mater Res Technol. 2024; 33:7136–46. https://doi.org/10.1016/j.jmrt.2024.11.082
2. Dias P., Lopes JG., Curado T., Maawad E., Schell N., Kim HS., Oliveira JP. In-situ microstructural

evolution during tensile loading of CoCrFeMnNi high entropy alloy welded joint probed by high energy synchrotron X-ray diffraction. Sci Technol Weld Join. 2024; 29:213–9. https://doi.org/10.1177/13621718241259349

3. Hernandez-Flores JE., Rodriguez-Vargas BR., Stornelli G., Miranda-Pérez AF., Di Schino A., Gómez-Casas J., García-Vázquez FDJ. Influence of the nickel powder addition in 308 stainless steel coatings on H13 tool grade steel. MRS Adv. 2024; 9:1891–5. https://doi.org/10.1557/s43580-024-00986-y
4. Mitelea I., Cosma D., Karancsi O., Burcă M., Crăciunescu CM., Uțu I-D. Hardfacing of GX-40CrNiSi25-20 cast stainless steel with an austenitic manganese steel electrode. Mater Test. 2024; 66:2055–65. https://doi.org/10.1515/mt-2024-0124
5. Świetlicki A., Walczak M., Szala M. Effect of shot peening on corrosion resistance of additive manufactured 17-4PH steel. Mater Sci-Pol. 2022; 40:135–51. https://doi.org/10.2478/msp-2022-0038
6. Szala M., Łukasik D. Pitting Corrosion of the Resistance Welding Joints of Stainless Steel Ventilation Grille Operated in Swimming Pool Environment. Int J Corros. 2018; 2018:1–7. https://doi.org/10.1155/2018/9408670
7. Szczucka-Lasota B., Węgrzyn T. Improvement of the mechanical properties of mobile platform stainless construction elements. Transp Probl. 2022; 17:91–102. https://doi.org/10.20858/tp.2022.17.4.08
8. Surkar HS., Kumar A., Sirohi S., Pandey SM., Świerczyńska A., Fydrych D., Pandey C. A dissimilar welded joint of grade 92 steel and AISI 304L steel obtained using IN82 buttering and IN617 filler: relationship of microstructure and mechanical properties. Arch Civ Mech Eng. 2024; 24:109. https://doi.org/10.1007/s43452-024-00920-x
9. Pańcikiewicz K., Radomski W. Lack of tightness analysis of concealed welded radiators. Eng Fail Anal. 2020; 114:104579. https://doi.org/10.1016/j.engfailanal.2020.104579
10. Janiczak R., Pańcikiewicz K. Laser welding of austenitic ferrofluid container for the KRAKsat satellite. Weld World. 2021; 65:1347–57. https://doi.org/10.1007/s40194-021-01103-5
11. Szala M., Beer-Lech K., Walczak M. A study on the corrosion of stainless steel floor drains in an indoor swimming pool. Eng Fail Anal. 2017; 77:31–8. https://doi.org/10.1016/j.engfailanal.2017.02.014
12. Orłowska M., Pańcikiewicz K., Świerczyńska A., Landowski M. Kinetics of intermetallic phase precipitation in manual metal arc welded duplex stainless steels. Materials. 2023; 16:7628. https://doi.org/10.3390/ma16247628
13. Tuz L., Sokołowski Ł., Stano S. Effect of post-weld heat treatment on microstructure and hardness of laser beam welded 17-4 PH stainless steel. Materials. 2023; 16:1334. https://doi.org/10.3390/ma16041334
14. Sirohi S., Pandey SM., Świerczyńska A., Rogalski G., Kumar N., Landowski M., Fydrych D., Pandey C. Microstructure and mechanical properties of combined GTAW and SMAW dissimilar welded joints between Inconel 718 and 304L austenitic stainless steel. Metals. 2022; 13:14. https://doi.org/10.3390/met13010014
15. Sonar T., Ivanov M., Trofimov E., Liu K., Shcherbakov I., Shaburova N., Samoilovskikh P. A critical review on dissimilar welding of ferritic-martensitic steel and austenitic stainless steel using gas tungsten arc welding process: Weldability issues, processing, and performance characteristics of joints. J Manuf Process. 2025; 133:811–64. https://doi.org/10.1016/j.jmapro.2024.11.081
16. Łastowska O., Starosta R., Jabłońska M., Kubit A. Exploring the potential application of an innovative post-weld finishing method in butt-welded joints of stainless steels and aluminum alloys. Materials. 2024; 17:1780. https://doi.org/10.3390/ma17081780
17. Coelho FGF., Bracarense AQ., Lima Ii EJ., Arias AR. Desenvolvimento de um modelo para parametrização do processo GMAW-P aplicado a manufatura aditiva por deposição a arco. Soldag Insp. 2024; 29:e2909. https://doi.org/10.1590/0104-9224/si29.09
18. Coelho FGF., Marinho LP., Arias AR., Silva AS. Avaliação da influência do magnetismo residual na soldagem GTAW de peças inspecionadas pelo método de partículas magnéticas. Soldag Insp. 2024; 29:e2906. https://doi.org/10.1590/0104-9224/si29.06
19. Toaldo PH., Ferreira ASF., Verastégui RN., Pukasiewicz AGM. Evaluation of the processing parameters influence on the additive manufacturing of VP50IM Steel by PCGTAW. Soldag Insp. 2024; 29:e2901. https://doi.org/10.1590/0104-9224/si29.01
20. Górka J., Jamrozik W., Wyględacz B., Kiel-Jamrozik M., Ferreira BG. Virtual sensor for on-line hardness assessment in TIG welding of Inconel 600 alloy thin plates. Sensors. 2024; 24:3569. https://doi.org/10.3390/s24113569
21. Alzahrani B., Ahmed MMZ., Habba MIA., Fouad RA., Elshaghoul YGY., Gadallah EA. TIG welding of EN AW-6082 Al alloy: A comparative analysis of filler rods on microstructural and mechanical performance. J Manuf Mater Process. 2025; 9:21. https://doi.org/10.3390/jmmp9010021
22. Sun Q., Liu Y., Kang K., Qian X., Liu C., Zhang Q., Sun Q. Morphology, mechanical property, and molten pool dynamics by narrow gap AMF-GTAW with swing filler wire. Sci Technol Weld Join. 2024; 29:319–27. https://doi.org/10.1177/13621718241273512

23. Abed Al Kareem SS., Mahdi BL., Hussein HK. Impact of TIG welding parameters on the mechanical properties of 6061-T6 aluminum alloy joints. Adv Sci Technol Res J. 2023; 17:114–29. https://doi.org/10.12913/22998624/171489
24. Karpagaraj A., Siva Shanmugam N., Sankaranarayanasamy K. Some studies on mechanical properties and microstructural characterization of automated TIG welding of thin commercially pure titanium sheets. Mater Sci Eng A. 2015; 640:180–9. https://doi.org/10.1016/j.msea.2015.05.056
25. Abima CS., Akinlabi SA., Madushele N., Akinlabi ET. Comparative study between TIG-MIG Hybrid, TIG and MIG welding of 1008 steel joints for enhanced structural integrity. Sci Afr. 2022; 17:e01329. https://doi.org/10.1016/j.sciaf.2022.e01329
26. Echezona N., Akinlabi SA., Jen TC., Fatoba OS., Hassan S., Akinlabi ET. Tig Welding of Dissimilar Steel: A Review. In: Awang M, Emamian SS, editors. Adv. Mater. Sci. Eng., Singapore: Springer Singapore; 2021; 1–9. https://doi.org/10.1007/978-981-16-3641-7_1
27. Bensaid N., Benlamnouar MF., Laib Dit Laksir Y., Saadi T., Badji R. Optimization of tungsten inert gas welding process parameters for joining austenitic stainless steel and copper using the Taguchi method. Adv Sci Technol Res J. 2024; 19:209–19. https://doi.org/10.12913/22998624/195449
28. Bhanu V., Fydrych D., Pandey SM., Gupta A., Pandey C. Activated tungsten inert gas weld characteristics of p91 joint for advanced ultra supercritical power plant applications. J Mater Eng Perform. 2024; 33:12070–82. https://doi.org/10.1007/s11665-023-08814-4
29. Vora J., Patel VK., Srinivasan S., Chaudhari R., Pimenov DY., Giasin K., Sharma S. Optimization of activated tungsten inert gas welding process parameters using heat transfer search algorithm: with experimental validation using case studies. Metals. 2021; 11:981. https://doi.org/10.3390/met11060981
30. He H., Tian X., Yi X., Wang P., Guo Z., Fu A., Zhao W. Optimization of joining parameters in pulsed tungsten inert gas weld brazing of aluminum and stainless steel based on response surface methodology. Coatings. 2024; 14:1262. https://doi.org/10.3390/coatings14101262
31. Saha S., Paul BC., Das S. Productivity improvement in butt joining of thick stainless steel plates through the usage of activated TIG welding. SN Appl Sci. 2021; 3:416. https://doi.org/10.1007/s42452-021-04409-7
32. Rao VA., Deivanathan R. Experimental investigation for welding aspects of stainless steel 310 for the process of TIG welding. Procedia Eng. 2014; 97:902–8. https://doi.org/10.1016/j.proeng.2014.12.365
33. Korinko PS., Malene SH. Considerations for the weldability of types 304L and 316L stainless steel. Pract Fail Anal. 2001; 1:61–8. https://doi.org/10.1007/BF02715336
34. Sun Z., Han H-Y. Weldability and properties of martensitic/austenitic stainless steel joints. Mater Sci Technol. 1994; 10:823–9. https://doi.org/10.1179/mst.1994.10.9.823
35. Costanza G., Sili A., Tata ME. Weldability of austenitic stainless steel by metal arc welding with different shielding gas. Procedia Struct Integr. 2016; 2:3508–14. https://doi.org/10.1016/j.prostr.2016.06.437
36. Durgutlu A. Experimental investigation of the effect of hydrogen in argon as a shielding gas on TIG welding of austenitic stainless steel. Mater Des. 2004; 25:19–23. https://doi.org/10.1016/j.matdes.2003.07.004
37. Varbai B. Shielding gas oxygen and nitrogen content effects in the case of duplex stainless steel welding. Adv Mater Sci. 2024; 24:111–23. https://doi.org/10.2478/adms-2024-0019
38. Iwaszko J., Strzelecka M. Microstructure and corrosion resistance of AZ91 magnesium alloy after surface remelting treatment. Materials. 2022; 15:8980. https://doi.org/10.3390/ma15248980
39. Nishad SK., Dwivedi DK. Influence of filler metal and arc pulsation on P91 steel weldments developed by activated TIG welding and its effect on stress corrosion cracking. Corros Sci. 2024; 239:112415. https://doi.org/10.1016/j.corsci.2024.112415
40. Szwajka K., Zielińska-Szwajka J., Trzepieciński T. The influence of the shielding-gas flow rate on the mechanical properties of TIG-welded butt joints of commercially pure grade 1 titanium. Materials. 2024; 17:1217. https://doi.org/10.3390/ma17051217
41. Mitru A., Semenescu A., Simion G., Scutelnicu E., Voiculescu I. Study on the weldability of copper – 304L stainless steel dissimilar joint performed by robotic gas tungsten arc welding. Materials. 2022; 15:5535. https://doi.org/10.3390/ma15165535
42. Rhode M., Erxleben K., Richter T., Schroepfer D., Mente T., Michael T. Local mechanical properties of dissimilar metal TIG welded joints of CoCrFeMnNi high entropy alloy and AISI 304 austenitic steel. Weld World. 2024; 68:1563–73. https://doi.org/10.1007/s40194-024-01718-4
43. Łyczkowska K., Adamiec J., Dolata AJ., Dyzia M., Wieczorek J. Regeneration of aluminum matrix composite reinforced by SiCp and GCsf using gas tungsten arc welding technology. Materials. 2021; 14:6410. https://doi.org/10.3390/ma14216410
44. Unnikrishnan R., Idury KSNS., Ismail TP., Bhadauria A., Shekhawat SK., Khatirkar RK., Sapate

SG. Effect of heat input on the microstructure, residual stresses and corrosion resistance of 304L austenitic stainless steel weldments. Mater Charact. 2014; 93:10–23. https://doi.org/10.1016/j.matchar.2014.03.013

45. Shankar V., Gill TPS., Mannan SL., Sundaresan S. Solidification cracking in austenitic stainless steel welds. Sadhana. 2003; 28:359–82. https://doi.org/10.1007/BF02706438
46. Luppo M i., Hazarabedian A., Ovejero-García J. Effects of delta ferrite on hydrogen embrittlement of austenitic stainless steel welds. Corros Sci. 1999; 41:87–103. https://doi.org/10.1016/S0010-938X(98)00083-3
47. García-García V., Reyes-Calderón F., Frasco-García OD., Alcantar-Modragón N. Mechanical behavior of austenitic stainless-steel welds with variable content of δ -ferrite in the heat-affected zone. Eng Fail Anal. 2022; 140:106618. https://doi.org/10.1016/j.engfailanal.2022.106618
48. Akbari Mousavi SAA., Miresmaeili R. Experimental and numerical analyses of residual stress distributions in TIG welding process for 304L stainless steel. J Mater Process Technol. 2008; 208:383–94. https://doi.org/10.1016/j.jmatprotec.2008.01.015
49. Ramon J., Basu R., Voort GV., Bolar G. A comprehensive study on solidification (hot) cracking in austenitic stainless steel welds from a microstructural approach. Int J Press Vessels Pip. 2021; 194:104560. https://doi.org/10.1016/j.ijpvp.2021.104560
50. Muthupandi V., Bala Srinivasan P., Seshadri SK., Sundaresan S. Effect of weld metal chemistry and heat input on the structure and properties of duplex stainless steel welds. Mater Sci Eng A. 2003; 358:9–16. https://doi.org/10.1016/S0921-5093(03)00077-7
51. Kumar S., Shahi AS. Effect of heat input on the microstructure and mechanical properties of gas tungsten arc welded AISI 304 stainless steel joints. Mater Des. 2011; 32:3617–23. https://doi.org/10.1016/j.matdes.2011.02.017
52. Ghumman KZ., Ali S., Khan NB., Khan MI., Ali HT., Ashurov M. Optimization of TIG welding parameters for enhanced mechanical properties in AISI 316L stainless steel welds. Int J Adv Manuf Technol. 2025; 136:353–65. https://doi.org/10.1007/s00170-024-14277-1
53. Ghumman KZ., Ali S., Din EU., Mubashar A., Khan NB., Ahmed SW. Experimental investigation of effect of welding parameters on surface roughness, micro-hardness and tensile strength of AISI 316L stainless steel welded joints using 308L filler material by TIG welding. J Mater Res Technol. 2022; 21:220–36. https://doi.org/10.1016/j.jmrt.2022.09.016
54. Wang J., Li J., Zong R. Influence of TIG process parameters on the microstructure and mechanical properties of 254SMO super austenitic stainless steel thin plate. Mater Today Commun. 2025; 44:111849. https://doi.org/10.1016/j.mtcomm.2025.111849